Research Square

Preprints are preliminary reports that have not undergone peer review.
They should not be considered conclusive, used to inform clinical practice,
or referenced by the media as validated information.

DNA methylation mediates the clonal transmission of a primed epigenetic state in a marine plant

Jessica Pazzaglia

jessica.pazzaglia@szn.it

Stazione Zoologica Anton Dohrn https://orcid.org/0000-0002-8677-7712

Luca Ambrosino

Stazione Zoologica Anton Dohrn https://orcid.org/0000-0003-1756-9538

Sandra Muñoz

Centro Oceanográfico de Murcia, Instituto Espanol de Oceanografia (IEO, CSIC)

Faustino Scarcelli

University of Calabria

Arantxa Ramos Segura

Centro Oceanográfico de Murcia, Instituto Espanol de Oceanografia (IEO, CSIC)

Emanuela Dattolo

Stazione Zoologica Anton Dohrn, 80121 Naples, Italy

Juan Ruiz

Centro Oceanográfico de Murcia, Instituto Espanol de Oceanografia (IEO, CSIC)

Gabriele Procaccini

Stazione Zoologica Anton Dohrn https://orcid.org/0000-0002-6179-468X

Lázaro Marín-Guirao

Centro Oceanográfico de Murcia, Instituto Espanol de Oceanografia (IEO, CSIC)
https://orcid.org/0000-0001-6240-8018

Article

Keywords:

Posted Date: August 5th, 2026

DOI: https://doi.org/10.21203/rs.3.rs-9943144/v1

License: This work is licensed under a Creative Commons Attribution 4.0 International License.
Read Full License

Additional Declarations: There is **NO** Competing Interest.

DNA methylation mediates the clonal transmission of a primed epigenetic state in a marine plant

Jessica Pazzaglia[1,2*], Luca Ambrosino[1], Sandra Muñoz[3], Faustino Scarcelli[4], Arantxa R. Segura[3], Emanuela Dattolo[1], Juan M. Ruiz[3], Gabriele Procaccini[1±], Lázaro Marín-Guirao[3±]

[1]Department of Integrative Marine Ecology, Stazione Zoologica Anton Dohrn, Villa Comunale, 80121, Naples, Italy

[2]National Biodiversity Future Center, 90133, Palermo, Italy;

[3]Centro Oceanográfico de Murcia, Instituto Espanol de Oceanografia (IEO, CSIC), 30740 San Pedro del Pinatar, Murcia, Spain

[4]Department of Chemistry and Chemical Technologies, Laboratory of Plant Biology and Plant Proteomics (Lab.Bio.Pro.Ve), University of Calabria, Rende 87036, Italy

*Corresponding author

[±]These authors have equally contributed

Abstract

Rapid environmental change poses severe threats to plant survival, requiring rapid and effective adaptive responses. The capacity to retain a molecular memory of past stress via epigenetic mechanisms has emerged as a key strategy to buffer climate variability. Clonality may facilitate such inheritance by preventing the epigenetic reprogramming typically associated with meiosis. Using the fast-growing pioneer seagrass *Cymodocea nodosa* as a model, we conducted a controlled thermal priming experiment to test whether heat-induced epigenetic modifications persist through clonal propagation and contribute to resilience under ocean warming. Following acute heat stress (35°C), high-resolution reduced representation bisulfite sequencing (RRBS-seq) revealed divergent epigenomic reprogramming despite comparable photophysiological buffering. Not-primed shoots exhibited a broad, reactive methylome reconfiguration consistent with stress-induced epigenetic resetting. In contrast, primed plants showed a constrained and energetically efficient response, characterized by targeted modulation and selective regulation of key regulatory hubs. Importantly, these stress-induced DNA methylation signatures persisted through clonal propagation into newly formed shoots, indicating stable vegetative transmission of epigenetic states. Our findings demonstrate that thermal priming establishes a preparatory, vegetatively transmitted epigenetic state, providing a critical proof-of-concept for assisted evolution strategies to actively mitigate climate impacts and sustain marine ecosystems.

1. Main text

Plants can retain a molecular "memory" of past environmental stresses, a phenomenon known as stress memory. This process is species-specific and depends on the duration, intensity, and recurrence of stress exposure [1]. Indications of stress memory transmission through sexual reproduction have been documented, suggesting that some DNA methylation marks can escape meiotic resetting and persist in offspring [2]. Nevertheless, growing evidence shows that stress memory can persist across generations also in clonal species [3,4]. Clonality, in fact, may offer an advantage for such inheritance, as the absence of meiosis during vegetative propagation prevents the epigenetic reprogramming that typically resets DNA methylation patterns, thereby allowing stress-induced epigenetic marks to be stably transmitted to new ramets [5]. The establishment of stress memory in plants requires multilevel reorganization across biological scales, involving coordinated biochemical, transcriptional, and epigenetic processes[6].

In this context, the heritability of stress memory and its trans-clonal transmission in plants has been primarily investigated through priming experiments. Exposure to sub-lethal stress can induce a persistent physiological state that modifies plant responses to subsequent stress events, thereby enhancing tolerance. This primed state is often mediated by epigenetic mechanisms and may result in sustained phenotypic plasticity across clonal generations. Research on plant memory is rapidly expanding, driven by the central ecological and economic roles of plants and by the accelerating environmental challenges to which plants are exposed. Understanding how plants naturally establish stress memory (e.g. vernalization[7]), and how such memory can be modulated through non-invasive approaches for improving performance (e.g. heat priming[8]), has become increasingly urgent.

Among plant groups with a distinctive evolutionary history are marine angiosperms, namely seagrasses, which recolonized coastal marine environments approximately 100 million years ago through multiple independent evolutionary events[9], and today underpin some of the most ecologically and economically valuable habitats on Earth [10]. Seagrasses are predominantly herbaceous clonal plants, and families such as Cymodoceaceae exhibit fast-turnover life-history strategies, contrasting with the slow-growing, long-lived forms characteristic of Posidoniaceae[11]. As a result of environmental changes and direct human impact, this group of marine plants is declining at alarming rates worldwide[12], with cascading effects on the stability and functioning of coastal ecosystems. Depending on stress type and species-specific plasticity, seagrasses can activate sophisticated stress-response mechanisms, including dynamic regulation of DNA methylation and transcription[13–16]. Through stable yet reversible modifications such as DNA methylation, epigenetic processes can modulate gene expression without altering the underlying DNA sequence, thereby mediating phenotypic plasticity in response to environmental changes [17]. Whether seagrasses retain memory of stress and inheritate response mechanisms across generations remains largely unexplored.

Here, we experimentally investigated the transmission of stress memory by performing a heat priming experiment in *Cymodocea nodosa,* a temperate fast-growing seagrass species. Its mixed sexual and clonal reproductive strategy, forming meadows of interconnected shoots linked by rhizomes, makes it an ideal system

to study trans-clonal inheritance. We tested whether heat-stress-induced epigenetic modifications can persist through clonal propagation and potentially contribute to adaptive resilience under ocean warming. By exposing shoots to sub-lethal heat stress and tracking DNA methylation patterns in their newly developed ramets, we assessed whether thermal stress imprints persist through vegetative growth, revealing potential mechanisms of epigenetic memory and resilience.

2. Material and Methods

2.1 Study species

Cymodocea nodosa forms mainly mono-specific meadows in shallow waters across the Mediterranean Sea and adjacent Atlantic coasts. It is considered a pioneer species due to its capacity to rapidly colonize bare sediment areas, facilitating the subsequent establishment of climax species such as *Posidonia oceanica*[18]. This species reaches its maximum growth rate in late spring and can colonize heterogeneous environments characterized by highly dynamic conditions, with fluctuations in temperature and salinity, such as lagoons [19]. *C. nodosa* can reproduce both sexually and vegetatively, with the balance between these modes of reproduction appearing to vary along a latitudinal gradient [20,21]. It exhibits a modular organization, in which the plant is composed of repeated ramets, each consisting of a shoot with leaves, roots, and a rhizome segment (**Fig. 1A**). These ramets are interconnected by horizontal rhizomes, contributing to clonal growth by enabling resource sharing and allowing apical shoots to expand horizontally and produce new ramets [22]. Highly genetically diverse meadows have been reported in regions characterized by high levels of sexual reproduction and seed production [23]. Meadows present an intermingled distribution of genets, with clonal patches reaching over 40 m in linear dimension [24,25]. Clonal integration plays a key role in the species' ecology and has been shown to be crucial for sustaining apical colonizing shoots (runners) under stress conditions [26]. Through physiological integration, resources such as nutrients and photosynthates can be translocated between neighboring ramets, allowing connected shoots to buffer local stress [27].

2.2 Sampling and mesocosm experiment

Sediment and horizontal rhizome fragments of similar size, bearing the apical shoot and 6-7 vertical shoots, were collected by SCUBA diving on May 02 2023 from a shallow (1.5m) monospecific meadow in the Mar Menor coastal lagoon (Spain, coordinates 37.771219, -0.755790). Fragments were extracted manually with great care to maximise integrity and minimize root damage.

Fragments were transplanted within 2 h into the mesocosm facility at the Oceanographic Center of Murcia (Spain), where the experiment was conducted. Each tank contained four rhizome fragments, which were carefully positioned in the sediment. A total of 12 independent indoor tanks (200 L each) were used, with four tanks assigned to each plant-condition (Primed, Not-Primed, and Control). Tanks were considered the true experimental units (n = 4 per treatment). While multiple shoots were measured for physiological and methylation analyses, replicate measurements within a tank were averaged to yield a single value per experimental unit. The mesocosm facility consists of a seawater capture system that collects seawater directly

from the Mar Menor lagoon through a dedicated intake system and filters and transports it to the experimental facility. Water circulation between the reservoir and experimental aquaria ensures continuous renewal and homogeneity of the aquatic environment across all experimental units. Water temperature is continuously monitored using digital temperature probes and data-loggers installed in both the main reservoir and the experimental tanks. Light conditions are provided using LED lighting systems with adjustable intensity and programmable photoperiods. The detailed description of the mesocosm system is provided in the Supplementary information (**Supplementary Methods and Fig. S1**).

Plants were pre-acclimated to the mesocosms under the environmental conditions matching those in the field at the time of collection. These conditions consisted of a temperature of 25 °C, salinity of 43 (practical salinity units), and a maximum irradiance of 200 µmol photons m^{-2} s^{-1} at canopy height under a 14 h:10 h light :dark photoperiod. The light cycle started at 07:00, with irradiance gradually increasing to a maximum at 12:30, maintained for 3 h, and then progressively decreasing until darkness at 21:00. Following this, the temperature was gradually increased at a rate of 1 °C day-1 in all tanks to reach the experimental control temperature of 28 °C, which corresponds to the natural warming rate observed in late spring/early summer in the region [2]. The pre-acclimation and acclimation phases lasted a total of 10 days. After the acclimation period, temperature was increased at a rate of 2°C per day in four tanks assigned to the priming (P) condition, until reaching 34°C. This maximum temperature was maintained for an additional 4 days, after which the temperature was gradually reduced back to the control level (28°C). The priming phase lasted a total of 8 days (**Fig. 1B**). *C. nodosa* shoots present during the priming period in primed, not-primed, or control conditions were referred to as "old-shoots" to distinguish them from those that developed after priming, hereafter referred to as "new-shoots". Plants were maintained under control conditions, and the apical shoot was marked with a cable tie to identify the last shoot exposed to priming. The subsequent growth phase was maintained for a period of 37 days, allowing the development of new shoots. Then, primed plants (P) and four additional tanks containing not-primed plants (NP) were exposed to the triggering stimulus. This treatment was designed to test priming acquisition and the transmission of stress memory from Old-Shoots to New-Shoots. Temperature was increased to 35°C, and plants remained exposed to this maximum temperature for 10 days before sampling. At this stage, leaf samples were collected from old and new shoots across different treatments (**Fig. 1B**).

2.3 Plant traits

Shoot number per rhizome was assessed across rhizomes weekly throughout the experiment to identify changes in shoot production in response to treatments. The Shoot Production Rate (SPR) was calculated by normalizing the number of new shoots produced over the time period. The result was expressed as the number of shoots produced per plant per day. At the end of the triggering phase, corresponding to the end of the experiment, entire rhizomes were harvested and weighed to determine their fresh weight. In addition, shoots and roots were separated and weighed individually in order to quantify their respective fresh biomass.

Photosynthetic performance was estimated by chlorophyll fluorescence using a Diving-PAM portable fluorometer (Walz, Germany). During the triggering event, maximum (Fm) and minimum (Fo) fluorescence

of dark-adapted leaves were measured to calculate the maximum quantum yield of PSII (Fv/Fm = (Fm − Fo)/Fm). Rapid light curves (RLCs) were performed at noon (after 4 h of illumination) using nine incremental irradiances (0, 13, 56, 134, 181, 280, 416, 655, and 830 µmol photons m^{-2} s^{-1}), each applied for 20 s.

Rapid light curves (RLCs) were fitted using the Regression II model implemented in WinControl (Walz) based on Platt, Gallegos and Harrison (1980)[29], from which ETR_{max} was derived. Absolute electron transport rates were calculated by incorporating leaf absorptance (A), estimated following Vásquez-Elizondo et al. (2017)[30]. Incident (L_o) and transmitted irradiance (L_t) were measured using the Diving-PAM miniature quantum sensor mounted on the leaf clip holder, and transmittance was calculated as $T = L_t/L_o$. Absorptance was estimated as $A = 1 - T$ after correction using bleached leaves as reference material. Non-photochemical quenching (NPQ) was calculated using maximum fluorescence of dark-adapted leaves (Fm) and light-adapted leaves (Fm′) according to the equation $NPQ = (Fm - Fm') / Fm'$. Oxygen exchange measurements were conducted at the end of the triggering phase to assess the photosynthetic O_2 production and dark respiration rates of *C. nodosa* leaves. Dissolved oxygen was measured non-invasively using a fiber-optic oxygen meter (Fibox 4, PreSens GmbH, Regensburg, Germany) coupled with oxygen-sensitive spots (PSt3) attached to the inner wall of airtight glass incubation chambers [31,32]. The system was calibrated using a two-point calibration (0% and 100% air saturation), with automatic compensation for temperature and salinity. Leaf segments were incubated in filtered seawater under controlled experimental conditions. For each treatment and shoot type, five epiphyte-free leaf segments were placed in individual chambers, and an additional chamber without plant material was used as a blank to account for background oxygen variation. Net photosynthesis was measured under constant irradiation (180 µmol photons m^{-2} s^{-1}) for 30 minutes, with oxygen concentration recorded every 5 min. Subsequently, chambers were darkened, and respiration rates were measured after a 10 min dark acclimation period over 40 min, using the same temporal resolution. Oxygen fluxes were calculated from the linear change in O_2 concentration over time, corrected by the blank and normalized to incubation volume and leaf surface area. Photosynthetic (Pmax) and dark respiration (DR) rates were expressed as µmol O_2 h^{-1} cm^{-2}. Photosynthetic pigments were extracted from leaf tissue in an 80% acetone buffered with $MgCO_3$ and incubated in the dark at 4 °C for 24 h. Extracts were then centrifuged (1000 g, 10 min,1 4 °C), and absorbance was measured at 470, 646, 663 and 725 nm using quartz cuvettes. Chlorophyll a, chlorophyll b and carotenoids were quantified following Lichtenthaler and Wellburn (1983)[33] and expressed on a biomass basis (µg/g).

2.5 DNA extractions and library preparation and sequencing

Genomic DNA was extracted from fresh leaf tissue randomly collected across treatments (control, primed, and not-primed; n = 5 per condition) and shoot type (new and old) at the end of the triggering phase. Samples were stored at -80°C prior to extraction, which was performed using the standard cetyltrimethylammonium bromide (CTAB) protocol (Doyle & Doyle, 1988). In brief, leaves were homogenized in 2 ml tubes containing tungsten beads. Cell lysis was initiated by adding 700 µl of CTAB buffer, followed by shaking using a Qiagen Tissue Lyser II for 5 minutes at 29 Hz. Samples were then incubated at 65°C for 10 minutes. To remove proteins, chloroform:isoamyl alcohol (24:1) was added, the mixture was thoroughly mixed, and then centrifuged at

13,000 g for 10 min. DNA was precipitated by adding an equal volume of isopropanol and incubating the samples at -20°C for 2 hours. Following the incubation, the samples were centrifuged at 13,000 rpm for 30 minutes at 7°C. The DNA pellet was washed twice with 95% and 70% ethanol. The dried pellets were then dissolved in pure water. DNA concentration and purity were assessed using the NanoDrop™ One UV-Vis Spectrophotometer and 1.0% agarose gel electrophoresis. Samples with purity values (260/280 ratio) higher than 1.8 were shipped on ice to the IGA technology services S.R.L. (Udine, Italy) for library preparation and sequencing. Ovation® RRBS Methyl-Seq (Tecan, Redwood City, CA) was used for library preparation following the manufacturer's instructions. Genomic DNA was digested using the TaqIα restriction enzyme (New England Biolabs, Ipswich, MA) following the manufacturer's recommended buffer conditions. Reactions were incubated at 65 °C for 2 hours to ensure complete digestion. A defined amount of unmethylated lambda DNA spike-in was included in each reaction to estimate the bisulfite conversion rate. Following the digestion step, reactions were heat-inactivated at 80 °C for 20 minutes and subsequently processed according to the downstream workflow requirements. Final libraries were checked with both Qubit 2.0 Fluorometer (Invitrogen, Carlsbad, CA) and Agilent Bioanalyzer DNA assay or Caliper (PerkinElmer, Waltham, MA). Libraries were then sequenced on paired-end 150 bp mode on NovaSeq6000 (Illumina, San Diego, CA). The number of reads (in millions) produced for each sample is listed in the Supplementary information (**Tab. S1**).

2.6 RRBS-seq analysis

RRBS-seq bioinformatics analysis was performed as follows. Base calling and demultiplexing of raw sequencing data were carried out using Illumina BCL Convert v3.9.3 for file format conversion and sample assignment. The Ovation RRBS-Seq System includes Unique Molecular Identifiers (UMIs) composed of eight random nucleotides to distinguish unique library molecules. UMI sequences, provided in the separate R2 FASTQ file, were incorporated into the headers of both R1 and R3 reads using umi_tools extract v1.1.1[34]. Illumina adapter sequences and low-quality bases were trimmed from raw FASTQ files using Trim Galore v0.6.6, with the parameter "-quality 20" (http://www.bioinformatics.babraham.ac.uk/projects/trim_galore/). Additional trimming of diversity bases was performed with a custom Python script provided by NuGen (Tecan).

Reads quality after preprocessing were assessed with FastQC v0.11.9 and individual reports were aggregated using MultiQC v1.9[35]. Reads were aligned to the reference genome of *P. oceanica* using Bismark v0.23.1, with the parameters "--bowtie2 e -N 1 --score_min 'L,0,-0.2' "[36], which enables mapping of bisulfite-converted reads and methylation calling in CpG, CHG, and CHH contexts. PCR duplicates were removed using umi_tools dedup v1.1.1[34], relying on UMI tags to identify redundant molecules.

Methylation calls for all cytosines in the three sequence contexts were generated using bismark_methylation_extractor v0.23.1 with the main parameters "--cytosine_report --CX_context --comprehensive --ignore 3 --merge_non_CpG". Methylation summary statistics and QC metrics were produced with bismark2report v0.23.1 and aggregated using MultiQC v1.11[35].

Differential methylation analysis (DMR) was conducted using the calculateDiffMeth function from the methylKit v0.9.5 package[37]. To explore the effect of priming, a first comparison was performed between treatments and controls for old shoot type at the end of the triggering phase (not_primed old vs control_old, 'primed_old vs control_old'). Then, to compare differences between shoots, DMRs were also obtained for the new shoot type ('primed_new vs control_new'). Additional contrasts across treatments and shoot types ('primed_new vs primed_old', 'not-primed_new vs not-primed_old') and within controls only ('control_new vs control_old') were included to investigate the inheritance of DNA methylation changes during clonal growth.

2.7 DMR annotation and GO enrichment

DMR annotation was performed using the *P. oceanica* reference genome[9], which includes structural gene models and annotated transposable elements (TEs). Genomic coordinates of the identified DMRs were intersected with these annotations using a custom Python workflow to classify DMRs according to genomic features (intergenic regions, promoter regions, gene bodies, and/or TEs). Protein-coding genes containing DMRs within their gene body or promoter region were subsequently subjected to functional annotation. For this purpose, predicted protein sequences were queried against the Swiss-Prot database[38] using BLASTx[39] with an E-value cutoff of 1e–3, retaining only the top-scoring hit to infer potential functional implications of methylation differences.

Gene Ontology (GO) enrichment analysis was performed using Ontologizer[40] to identify overrepresented functional categories among genes associated with differentially methylated regions (DMRs). DMRs were separated by sequence context (CG, CHG, CHH) and analyzed independently for new and old shoots. Enrichment was assessed with the Parent–Child Union method coupled with a hypergeometric test, and p-values were adjusted for multiple testing with the Benjamini–Hochberg false discovery rate (FDR). GO terms with FDR-adjusted p-value < 0.05 were considered significantly enriched.

2.8 DNA methylation visualization

Genome-wide DNA methylation profiles were summarized using a binning and normalization pipeline to enable quantitative comparison across experimental conditions and cytosine contexts (CG, CHG, CHH). Per-site methylation data obtained from methylKit were aggregated into non-overlapping 10 kb bins based on genomic coordinates, and coverage values were summed to generate context-specific methylation tracks for each condition. To facilitate genome-scale visualization, 10 kb bins were further aggregated into 50 kb non-overlapping windows. Within each cytosine context, methylation signals were normalized using a global maximum scaling approach, whereby values were rescaled to a 0–100 range relative to the maximum signal observed across all conditions and bins. This strategy preserves relative differences while allowing direct comparison among treatments. Normalized 50 kb tracks were exported in Circos-compatible format. Gene and transposable element densities were calculated using the same 50 kb binning scheme to ensure coordinate consistency. Circular genome plots were generated using Circos[41], with chromosomes represented as

ideograms and methylation levels displayed as concentric heatmaps. Logarithmic scaling was applied to enhance contrast while maintaining high-intensity signals.

2.9 Statistical analysis

To explore how primed and non-primed shoots (i.e. old shoots exposed or not exposed to the priming treatment) responded to the triggering event, a one-way ANOVA was performed considering only old shoots. In this analysis, plant condition was included as a fixed factor with three levels: primed, not-primed, and control. Differences between new and old shoots within each treatment (control, not-primed, primed) were assessed using Welch's two-sample t-tests, which do not assume equal variances. For each comparison, test statistics (t), degrees of freedom (df), p-values, means, and 95% confidence intervals were reported. To evaluate the combined effects of treatment and shoot type, two-way ANOVAs weres performed with Treatment (control, not-primed, primed) and Shoot type (New, Old) as fixed factors. When appropriate, post hoc comparisons were conducted, with statistical significance set at $p < 0.05$. Values of $0.05 < p < 0.1$ were considered indicative of trends. All analyses were conducted in R (version 4.3.2) using the *stats* and *dplyr* packages.

To test for significant changes in DNA methylation patterns, a two-way ANOVA was also performed using the same design as the one used for plant photo-physiological responses. In this analysis, differences in differentially methylated regions (DMRs) observed in CG, CHG, and CHH contexts were tested across treatments and shoot types. In addition, principal component analysis (PCA) was carried out to explore associations among photo-physiological traits.

3. Results and Discussion

Epigenetic regulation contributes to the capacity of *C. nodosa* to cope with rapid environmental change, supporting the presence of stress memory in this clonal marine plant. This was assessed through an integrated analysis of physiological measurements and DNA methylation patterns (**Figs. 2–4**), using a thermal priming approach to investigate stress memory in *C. nodosa* for the first time.

Exposure to the triggering treatment had significant effects in both primed and non-primed shoots, affecting not only photophysiology (**Fig. 3A**), but also in shoot production (**Fig. 3B**), and in genome-wide methylation patterns (**Fig. 4**). Treated plants displayed distinct physiological and epigenetic profiles compared to controls, with not-primed (NP) shoots showing stronger photo-physiological and methylation changes than primed (P) ones (**Fig. 3 and 4**). We first describe the methylome of *C. nodosa*, followed by the effects of priming and the potential role of clonal transgenerational epigenetic inheritance (clonal TEI).

The DNA methylation landscape of Cymodocea nodosa under thermal stress

DMRs were distributed across all chromosomes, forming distinct hotspots (**Fig. 2**). The predominance of CG methylation, followed by CHG and CHH contexts, is consistent with the hierarchical stability of plant methylation and suggests that stress-induced remodeling primarily affects the most stable epigenetic layer.

Methylation changes were more pronounced in old than in new shoots (**Fig. 2; Supplementary Tab. 2**), with stronger differences in DMRs observed in non-primed compared to primed plants. This pattern is consistent with studies in land plants showing that stress-induced methylation changes can persist across clonal generations, suggesting transgenerational phenotypic plasticity[42–44], and indicates that the priming treatment may have contributed to the maintenance of regulatory stability across shoots. Regions enriched in transposable elements (TEs) generally showed increased methylation, particularly in CG and CHG contexts (**Fig. 2**), whereas CHH methylation was more localized and dynamic. Under stress, TE-associated methylation may become more responsive, potentially influencing TE activity and adjacent gene regulation, thereby contributing to the establishment of stress memory across generations[45]. This pattern was especially evident in the CHH context, consistent with its known regulatory activity[46]. Across all sequence contexts, NP shoots exhibited approximately twice as many DMRs as P shoots (**Fig. 4**), indicating that in the absence of priming, heat stress induces broader methylome reconfiguration. In contrast, priming appears to constrain epigenomic variability, promoting a more controlled regulatory response.

Unlike previous observations in *P. oceanica*[47], *C. nodosa* did not display clear differences in the proportion of hypo- and hypermethylated regions between P and NP shoots (**Fig. 4B**). Moreover, whereas DMRs in *P. oceanica* were predominantly intergenic[47], in *C. nodosa* they were mainly located within gene bodies (i.e. intron/exon regions) (**Fig. 4A**). This suggests a distinct regulatory strategy based on gene body methylation (GbM), a conserved feature of plant genomes typically associated with moderately expressed genes[48]. In this context, GbM may support fine-tuned, gene-specific regulation rather than broad transcriptional shifts. Although the functional role of GbM remains debated in model systems (e.g. *Arabidopsis*[49]), in clonal marine plants such as *C. nodosa* it may contribute to stabilizing transcriptional output under recurrent stress, thereby supporting short- or long-term epigenetic memory. Such a mechanism may enhance resilience and fine-tune stress responses in dynamic coastal environments[50]. DMRs in the CG context were consistently abundant across several chromosomes (Chr01, Chr02, Chr03, and Chr07) in all treatments (**Fig. 2; Supplementary Tab. 3**), suggesting that these regions may represent genomic hotspots of epigenetic regulation. In contrast, other chromosomes, such as Chr08, Chr12, and Chr18, showed pronounced increases in DMRs specifically in NP new shoots (**Fig. 2; Supplementary Fig. 2; Supplementary Tab. 3**), diverging from the pattern observed under P conditions and suggesting a more dynamic and treatment-dependent regulation. Supporting this, regions on Chr 12 and 18 included DMRs associated with basal heat stress responses shared across conditions, whereas genes involved in stress signaling and environmental responsiveness, such as intracellular transporters (*AP-4 complex*), ion channels (*CNGC1*), kinesin-related proteins, and universal stress proteins, were specifically regulated in NP shoots.

Priming targets DNA methylation without altering photosynthetic performance

To determine whether priming enhances stress responses, we analyzed the photophysiology and DNA methylation in old shoots after the triggering phase (**Supplementary Tabs. 4-6**). Despite exposure to the thermal stress, key photophysiological parameters (abs-ETRmax, Fv/Fm, pigment content, Pmax) remained

stable, whereas dark respiration (DR) increased in both primed (P) and non-primed (NP) shoots, leading to reduced Pmax/DR ratios (**Fig. 3A; Supplementary Fig. 3; Supplementary Tab. 4**). As a consequence of increased respiratory demand, the decline in Pmax/DR reflects a shift in leaf carbon balance, indicating higher metabolic costs under stress. Such buffering of thermal stress has been previously reported in *C. nodosa,* where declines in photosynthetic performance occur only after several days of recovery under lower temperatures[51]. Together, these results suggest that this species can withstand transient thermal stress through short-term physiological compensation, while prolonged exposure may ultimately impair photosynthetic function.

In our priming experiment, shoots exposed to repeated stress (priming followed by triggering) did not exhibit detectable photophysiological differences compared to NP shoots. Rather than enhancing performance, priming appears to stabilize it, preventing additional stress-induced damage to the photosynthetic apparatus. In contrast, DNA methylation revealed distinct regulatory strategies. NP shoots showed widespread methylation changes across all sequence contexts, affecting genes involved in mitochondrial respiration (*ND2*, *COQ6*), protein modification (according to GO terms, GO:0140640, GO:0032991), and oxidoreductase activity (GO:0016661),consistent with increased metabolic demand (**Supplementary Tab. 7; Supplementary Data 1-3**). Among the most hypomethylated CG-DMRs, several were associated with genes involved in protein synthesis (*coq6*, encoding ubiquinone biosynthesis monooxygenase COQ6, mitochondrial), stress protection (*HSP18.2*, encoding a 18.2 kDa class I heat shock protein), mitochondrial function (*IscA2*, encoding an iron-sulfur assembly protein IscA-like 2, mitochondrial), and epigenetic regulation (*HDAC1*, encoding histone deacetylase 1) (**Supplementary Data 1**). Conversely, genes involved in mitochondrial respiration (*ND2*), flavonoid biosynthesis (*flavonoid 3'-monooxygenase*), and protein translation (*GluRS*), exhibited promoted hypermethylation. These patterns suggest that NP shoots may rely on a broad and reactive stress response, potentially reflecting the absence of prior conditioning. By contrast, P shoots exhibited fewer but more functionally targeted methylation changes, involving genes linked to chloroplast function (*PTAC10*), transcriptional regulation (*MED15A*), stress detoxification (*Sacs*), and ribosome assembly (GO:0030684, preribosome) that were among the most hypo-methylated (**Supplementary Tab. 7; Supplementary Data 1**). By selectively modulating key regulatory hubs rather than the entire metabolic machinery, P shoots avoid the energetic drain of a generalized stress response. This suggests that priming establishes a preparatory epigenetic state that enables controlled regulation while minimizing energetic costs.

Although most DMRs occurred in the CG context (**Fig. 2, 4A; Supplementary Fig. 4A-B**), a subset was detected in the CHG context, which is known to be particularly responsive to environmental stress in plants[52]. High CHG methylation has also been reported in *P. oceanica*[47] and *Zostera marina*[53], suggesting a conserved role in environmental responsiveness across seagrasses. In both CG and CHG contexts, P shoots displayed hypomethylation of genes involved in the Mismatch Repair (MMR), Homologous Recombination (HR) machinery, and cellular homeostasis. Notably, *RAD51* (DNA repair protein homolog 4) and *MSH4* (DNA mismatch repair protein), key components of homologous recombination and DNA repair pathways, were hypomethylated within gene bodies (~ - 35%), whereas *MLH1* (DNA mismatch repair protein), *IMP3* (U3 small nucleolar ribonucleoprotein protein) and *PAP26* (Bifunctional purple acid phosphatase 26), showed

promoter hypomethylation (-32%, ~ - 45%, -25% respectively; **Supplementary Data 1 - 2**). This distribution suggests distinct regulatory mechanisms acting on functionally related genes. By reducing methylation levels at these loci, priming effectively lowers the transcriptional activation threshold for the repair system, creating a "ready-to-act" state. In contrast, NP shoots the mitochondrial mismatch repair protein MSH1 experienced heavy hypermethylation (+57.5%) suggesting a late stage functional reorganization to oxidative stress where NP invested in reactive survival. Given that gene body methylation is often associated with stable gene expression[54], whereas promoter methylation typically regulates transcriptional activation, these patterns may support both transcriptional competence and regulatory flexibility. Such coordinated modulation of genome maintenance pathways is consistent with the establishment of a preparatory epigenetic state associated with stress-memory. Similar patterns have been described in *P. oceanica,* where thermal priming affects DNA repair–related genes[47], and more broadly across plant systems[55,56].

In NP shoots, promoter hypomethylation of *POLR3D* (DNA-directed RNA polymerase III subunit RPC4) and gene body hypermethylation of *RAD50* (DNA repair protein) and *ALKBH2* (DNA oxidative demethylase) further support a reactive transcriptional strategy. *POLR3D* is essential for RNA Polymerase III function and the synthesis of tRNAs and 5S rRNA[57], its hypomethylation may enhance transcriptional activity to meet increased metabolic demands under acute stress[58]. The absence of similar changes in P shoots suggests that primed plants may avoid such costly transcriptional upregulation by maintaining a pre-conditioned regulatory state. In addition, reduced methylation of *ALKBH2* in NP shoots may reflect activation of DNA repair pathways to protect genomic integrity under thermal stress[59].

Few DMRs were shared between the P and NP shoots, and those that were shared generally exhibited similar methylation levels, likely representing core heat stress responses (**Supplementary Fig. 5**). However, some genes showed opposite methylation patterns between treatments, indicating priming-dependent regulatory divergence (**Supplementary Data 4**). For example, *NUP188* (Nucleoporin) and *EDD1* (Protein EMBRYO-DEFECTIVE-DEVELOPMENT 1) were hypomethylated in P but hypermethylated in NP shoots, potentially reflecting enhanced transport and proteostasis under priming. Conversely, *PKL* (CHD3-type chromatin-remodeling factor PICKLE) and *NRPD1* (RNA polymerase IV subunit 1) were hypermethylated in P and hypomethylated in NP, suggesting selective repression of chromatin remodeling pathways in primed plants. In the CHG context, only one DMR showed opposing methylation patterns: *KAPP* (Protein phosphatase 2C 70) , a conserved and protein phosphatase involved in phosphorylation homeostasis[60], was hypermethylated in P and hypomethylated in NP. Overall, these results support the view that priming acts as an epigenetic buffering mechanisms, shifting the plant response from a broad, reactive strategy to a more controlled and potentially energy-efficient regulatory program

Physiological and epigenetic responses across clonal shoots

To evaluate clonal transgenerational epigenetic inheritance**,** we compared responses between new and old shoots within each treatment (**Fig. 1, Fig. 2; Supplementary Tabs. 4-5**). The persistence of stress memory

across clonal shoots was trait-dependent, expressing more clearly at the metabolic than at the photochemical level**.** Pigments composition (chlorophyll *a* and *b*) and NPQ were significantly influenced by shoot type but not by treatment**,** suggesting that ontogenetic regulation overrides priming history in shaping structural and photoprotective traits (**Fig. 3C; Supplementary Tab. 4**). Likewise, Fv/Fm and abs-ETRmax were largely unaffected by treatment, indicating that core PSII efficiency and electron transport capacity are not detectably transmitted to newly formed clonal shoots (**Supplementary Fig. 1; Supplementary Tab. 4**). Two-way ANOVA confirmed the absence of a significant Treatment × Shoot interaction for these variables**,** reflecting comparable responses across shoot types (**Supplementary Tab. 4**). This physiological pattern was mirrored by the analysis of DNA methylation, where no significant interaction between Treatment and Shoot was detected across CG and CHG (**Supplementary Tab. 2**). In the CG context, clear differentiation between primed and non-primed conditions occurred within each shoot type, with the number of DMRs nearly doubling between treatments (**Fig. 4A-C; Supplementary Fig. 4A-B**). Significant differences were also detected both between shoot types and treatments (**Supplementary Tab. 2**). CHG methylation varied primarily between shoot types within the same treatment, particularly under non-primed conditions, where the number of unique DMRs increased approximately threefold from old and new shoots (**Fig. 4C**). In contrast, the CHH context exhibited a significant Treatment × Shoot interaction, highlighting it as a dynamic site for shoot-specific priming responses.

The developmental stage is known to influence plant responses to environmental stress, affecting both physiological performance and genome-wide regulatory processes[61,62]. In this study, the higher pigment content in new shoots compared to old ones likely reflects clonal integration, where older modules physiologically support younger ones to buffer environmental variability. In seagrasses, such integration is a key mechanism supporting performance and resilience under environmental variability[63,64]. Interestingly, these differences were significant mainly in primed shoots (**Supplementary Tab. 4**), suggesting that priming influences resource allocation or physiological connectivity along the rhizome. Conversely, dark respiration (Rd) showed a robust, consistent treatment effect, increasing under heat stress across both shoot types (**Fig. 1A; Supplementary Tab. 6**). The resulting decrease in Pmax/Rd reflects this respiratory rise indicating a shift in carbon balance toward higher metabolic expenditure. The persistence of this respiratory pattern in new shoots suggests a systemic physiological adjustment along the rhizome, consistent with clonal propagation of stress effects. Because respiration integrates carbon balance and cellular energy status, its modulation appears to be a central component of stress memory in seagrasses. Consistent with this interpretation, shoot production rate (SPR) increased significantly under priming (**Fig. 3B; Supplementary Tab. 8**), suggesting that these metabolic adjustments translate into enhanced clonal growth and expansion. In seagrasses, shoot production is a key mechanism for meadow persistence and expansion[65], indicating that priming-induced reprograming has functional ecological consequences.

Epigenetic transmission of stress memory in clonal shoots reveals context-specific gene targets

A detailed analysis of differentially methylated regions (DMRs) revealed patterns of stability and regulation consistent with a context-dependent transmission of stress memory across clonal shoots. Despite the absence of global differences in CG methylation levels, between treatments and shoot types, several gene body DMRs were shared across conditions (**Fig. 4; Supplementary Data 4**). Most of these regions displayed conserved methylation patterns, suggesting constitutive epigenetic regulation in *C. nodosa* under thermal stress. Among these, genes associated with the Nuclear Pore Complex (NPC) showed contrasting methylation patterns between treatments. NUP188, previously identified in old shoots, was hypermethylated in primed (P) shoots and hypomethylated in not-primed (NP) shoots. (**Supplementary Data 4**) Similarly, *NUP205* and *NLGase* were shared between conditions but exhibited opposite methylation patterns in new shoots, being hypermethylated in NP and hypomethylated in P shoots. Notably, P new shoots showed hypomethylation of genes directly associated with the NPC core (*NUP205*), as well as genes functionally linked to nuclear transport through the MOS4-associated complex and importin pathways (e.g., *MOS4* and *MOS14*). Given the central role of NPC in regulating RNA/protein trafficking during abiotic stress[66], these patterns suggest that nuclear transport pathways may be selectively targeted by priming. Such regulation should facilitate a more coordinated and efficient stress response in newly formed shoots.

While priming promoted a highly consistent and stabilized epigenetic landscape across developmental stages, the absence of priming led to a more reactive, variable, and uncoordinated regulatory response. This contrast is evident when comparing DMRs between new and old shoots under P and NP conditions. Although both conditions shared a comparable number of DMRs across shoot types (**Fig. 4C; Supplementary Data 4**), NP shoots exhibited pronounced epigenetic instability, with several loci showing strictly opposite methylation trends between developmental stages. Specifically, genes genes critical for stress adaptation, including hose mediating oxygen responses (*NAR1*), protein transport (*AtVAMP726*), and abscisic acid regulation (*AtDPBF4*), were hypermethylated in new shoots but hypomethylated in old shoots (**Supplementary Data 4**). Conversely, the intermembrane lipid transfer protein gene *vps13A* displayed the inverse pattern. Analysis of unique DMRs further highlighted contrast regulatory strategies. NP new shoots showed extensive methylation changes across genes involved in metabolism and transport, including NAD-dependent malic enzyme (*NAD-ME*), *Sec61*, and RNA methyltransferases, consistent with a broad and dynamic epigenetic response (**Supplementary Data 4**). In contrast, P new shoots exhibited highly targeted methylation changes directed toward functional refinement. Genes such as Ferritin-3 (*SFerH*-3) and Protochlorophyllide-dependent translocon component 52 (*PDT52*), were hypermethylated in their promoter and intron/exon regions respectively, suggesting fine-tuned regulation of iron storage and chloroplast protein import tightly linked to the oxidative balance of plastid function[67]. At the same time, several metabolic and photosynthesis-related genes (i.e., Uridine kinase-like protein 1, Ribulose-5-phosphate-3-epimerase, PsbP domain-containing protein 2) were predominantly hypomethylated. These patterns are consistent with the maintenance of photosynthetic capacity, pigment accumulation, and ion homeostasis observed in new shoots (**Fig. 3; Supplementary Fig. 1; Supplementary Tabs. 4-5**). These epigenetic adjustments likely optimize the energetic and metabolic demands required for increased shoot

production, providing a mechanistic link between priming-induced methylation changes and the observed responses in terms of photosynthetic performance and growth.

In the CHG context, shared DMRs between shoots generally showed stable methylation levels (**Supplementary Data 4**), Conversely, NP shoots exhibited broader regulation involving genes associated with epigenetic and chromatin remodeling (*HDA5*, Histone deacetylase 5), DNA replication (*POL2A*, DNA polymerase epsilon catalytic subunit A), and stress signaling (e.g., *DAG*, Diacylglycerol kinase 1). By contrast, P new and old shoots shared DMRs enriched in components of the RNA-directed DNA methylation (RdDM) pathway, including DNA (cytosine-5)-methyltransferase (DRM2) and RNA polymerase V. The targeted involvement of RdDM-related genes suggests that priming may promote coordinated epigenetic regulatory networks across developmental stages. In plants, the canonical RdDM pathway mediates *de novo* DNA methylation, via small RNA-guided targeting, playing a documented role in regulating stress responsive genes and epigenetic memory [6869]. While these patterns indicate that small RNA-mediated mechanisms may serve to stabilize seagrass stress memory, the functional dynamics of RNA-directed epigenetic regulation in these marine angiosperms remain largely unexplored. Finally, CHH context DMRs were predominantly enriched in NP old shoots, which exhibited the highest number of epigenetic changes. These DMRs were mainly associated with genes involved in stress signaling (*MLO5*, MLO-like protein 5), transport (*ABCC13*, ABC transporter C family member 13), and metabolic regulation (*RCA1*, Ribulose bisphosphate carboxylase/oxygenase activase, chloroplastic) (**Fig. 4C; Supplementary Data 4**), consistent with a more dynamic and stress-responsive epigenomic landscape.

Together, these results indicate that the epigenetic transmission of stress memory in clonal shoots is strongly context-dependent. Specifically, CG methylation appears to encode the baseline priming-related memory, CHG reflects coordinated regulation across shoot ontogeny, and CHH captures dynamic, stress-responsive fluctuations.

Epigenetic stability supports memory transmission during clonal growth

When DMRs were analyzed by comparing methylation patterns between new and old shoots within the same treatment, evidence of epigenetic stability across clonal modules emerged. To disentangle treatment effects from development variation, control conditions were included to identify shared and condition-specific DMRs. Most DMRs were detected under NP conditions (**Fig. 5A**), with no marked differences in hyper- and hypomethylation levels among treatments compared with the control (**Fig. 5B**). Only a single DMR was shared across all conditions (**Fig. 5C; Supplementary Fig. 3; Supplementary Data 5**), highlighting the high specificity of methylation responses. Notably, primed (P) shoots displayed greater epigenetic stability, particularly in CG and CHG contexts, where hypermethylated DMRs predominated (**Supplementary Data 1-3**). These regions were associated with genes involved in translation, meiosis, nutrient storage, and intracellular transport, suggesting sustained regulation of pathways linked to cell proliferation and biomass accumulation, consistent with increased rhizome growth (**Supplementary Data 5**).

In contrast, not-primed (NP) shoots exhibited extensive methylation reconfiguration. This was particularly pronounced in the CG context, where numerous DMRs showed strong hypo- and hypermethylation relative to old shoots (**Supplementary Fig. 3A-B**). Affected genes included those involved in transport (>90% hypomethylation; *CAT9*, cationic amino acid transporter 9, chloroplastic), chromatin regulation (>70% hypomethylation; *HDAC1*, histone deacetylase 1), and stress responses (>50% hypomethylation; *HSP18.2*, 18.2-kDa class I heat shock protein; >70% hypomethylation; *NAR1*), indicating a broad and reactive epigenetic response. Similarly, in the CHG context, genes such as *DTX46* (protein detoxification 46, chloroplastic), *FES1* (FRIGIDA-essential 1), and *PAS2* (very-long-chain (3R)-3-hydroxyacyl-CoA dehydratase PASTICCINO 2) were strongly hypomethylated in new shoots (>60% hypomethylation), pointing to regulation of developmental processes, stress responses, and organelle function. These pathways are typically associated with primary metabolism and nitrogen processing in actively growing tissues[70].

A subset of DMRs shared between P and NP shoots showed opposite methylation patterns, reinforcing the divergence between primed and non-primed regulatory strategies (**Fig. 5D; Supplementary Data 5**). For example, *YSL12* (probable metal–nicotianamine transporter), *RED1* (short-chain dehydrogenase), and *KAPP* (protein phosphatase 2C 70) were hypermethylated in P shoots but hypomethylated in NP shoots. Comparisons with control conditions confirmed that these patterns were treatment-specific rather than driven by ontogenic differences.

Ecological Relevance and Conclusion

Our results show that DNA methylation dynamics provide a mechanistic basis for stress memory in the clonal seagrass *Cymodocea nodosa*, and possibly in seagrasses in general. Priming establishes a preparatory epigenetic configuration that stabilizes regulatory pathways involved in metabolism, transport, and genome maintenance, enabling plants to maintain physiological performance under repeated thermal stress. Rather than enhancing photosynthetic capacity, priming appears to optimize the balance between carbon gain and metabolic demand, supporting sustained growth and clonal expansion. This is consistent with the observed increase in shoot production and the modulation of respiratory processes, highlighting metabolism as a central component of stress memory. Transmission of stress memory was more evident at metabolic and epigenetic levels than at the photochemical level, indicating selective propagation of stress effects across clonal modules. From an ecological perspective, such epigenetic plasticity may enhance the resilience and persistence of seagrass meadows under increasing environmental variability. By maintaining growth and clonal expansion under recurrent stress, primed plants may help maintain key ecosystem functions, including carbon sequestration, sediment stabilization, and habitat provision. Overall, these findings support the idea that epigenetic regulation contributes to the capacity of clonal marine plants to cope with rapid environmental changes and highlight DNA methylation as a key mechanism linking past environmental exposure to future stress responses.

References

1. Cañizares, E., Giovannini, L. & González-guzmán, M. Seeds of Change : exploring the transformative effects of seed priming in sustainable agriculture. 1–16 (2025) doi:10.1111/ppl.70226.

2. Ramakrishnan, M. *et al.* Epigenetic stress memory: A new approach to study cold and heat stress responses in plants. *Front. Plant Sci.* **13**, 1075279 (2022).

3. Nishad, A. & Nandi, A. K. Recent advances in plant thermomemory. *Plant Cell Rep.* **40**, 19–27 (2021).

4. Bruce, T. J. A., Matthes, M. C., Napier, J. A. & Pickett, J. A. Stressful 'memories' of plants: Evidence and possible mechanisms. *Plant Sci.* **173**, 603–608 (2007).

5. Ibañez, V. N. & Quadrana, L. Shaping inheritance: how distinct reproductive strategies influence DNA methylation memory in plants. *Curr. Opin. Genet. Dev.* **78**, 102018 (2023).

6. Aswathi, K. P. R. *et al.* The Plant Mind: Unraveling Abiotic Stress Priming, Memory, and Adaptation. *Physiol. Plant.* **177**, e70372 (2025).

7. Sung, S. & Amasino, R. M. Vernalization and epigenetics: How plants remember winter. *Curr. Opin. Plant Biol.* **7**, 4–10 (2004).

8. Zhang, X., Rossi, S., Zhuang, L., Dodd, I. C. & Huang, B. Stress priming mechanisms that enhance plant high temperature tolerance. *Environ. Exp. Bot.* **237**, 106208 (2025).

9. Ma, X. *et al.* Seagrass genomes reveal ancient polyploidy and adaptations to the marine environment. *Nat. Plants 2024* 1–16 (2024) doi:10.1038/s41477-023-01608-5.

10. Costanza, R. *et al.* The value of the world's ecosystem services and natural capital. *Nature* **387**, 253–260 (1997).

11. Larkum, A. W. ., Orth, R. J. & Duarte, C. M. *Seagrasses: Biology, Ecology and Conservation*. *Springer* vol. 53 (2006).

12. Waycott, M. *et al.* Accelerating loss of seagrasses across the globe threatens coastal ecosystems. *Proc. Natl. Acad. Sci.* **106**, 12377–12381 (2009).

13. Pazzaglia, J. *et al.* DNA methylation dynamics in a coastal foundation seagrass species under abiotic stressors. *Proc. R. Soc. B Biol. Sci.* **290**, 20222197 (2023).

14. Pazzaglia, J. *et al.* Handling the heat: ocean acidification mitigates the effects of marine heatwaves on Posidonia oceanica seedlings . *J. Exp. Bot.* **00**, 1156–1171 (2025).

15. Pazzaglia, J. *et al.* Local environment modulates whole-transcriptome expression in the seagrass

Posidonia oceanica under warming and nutrients excess. *Environ. Pollut.* **303**, 119077 (2022).

16. Nguyen, H. M. *et al.* Stress memory in seagrasses: first insight into the effects of thermal priming and the role of epigenetic modifications. *Front. Plant Sci.* **11**, 494 (2020).

17. Pazzaglia, J., Reusch, T. B. H., Terlizzi, A., Marín-Guirao, L. & Procaccini, G. Phenotypic plasticity under rapid global changes: The intrinsic force for future seagrasses survival. *Evol. Appl.* **00**, 1–21 (2021).

18. Borum, J., Duarte, C. M., Krause-Jensen, D. & Greve, T. M. European seagrasses: an introduction to monitoring and management. at https://pure.au.dk/portal/en/publications/european-seagrasses-an-introduction-to-monitoring-and-management/ (2004).

19. Ramfos, A. *et al.* Ecological and environmental characteristics of a seagrass-dominated hypersaline coastal Mediterranean lagoon: a multidisciplinary approach. *Aquat. Sci.* **86**, 1–16 (2024).

20. Tuya, F. *et al.* Seagrass Cymodocea nodosa across biogeographical regions and times : Differences in abundance , meadow structure and sexual reproduction. **162**, (2020).

21. Ruocco, M., Jahnke, M., Silva, J., Procaccini, G. & Dattolo, E. 2b-RAD Genotyping of the Seagrass Cymodocea nodosa Along a Latitudinal Cline Identifies Candidate Genes for Environmental Adaptation. *Front. Genet.* **13**, 866758 (2022).

22. Procaccini, G., Olsen, J. L. & Reusch, T. B. H. Contribution of genetics and genomics to seagrass biology and conservation. *J. Exp. Mar. Bio. Ecol.* (2007) doi:10.1016/j.jembe.2007.05.035.

23. Máñez-Crespo, J. *et al.* Seagrass Cymodocea nodosa across biogeographical regions and times: Differences in abundance, meadow structure and sexual reproduction. *Mar. Environ. Res.* **162**, (2020).

24. Ruggiero, M. V., Capone, S., Pirozzi, P., Reusch, T. B. H. & Procaccini, G. Mating system and clonal architecture: A comparative study in two marine angiosperms. *Evol. Ecol.* **19**, 487–499 (2005).

25. Ruggiero, M. V., Reusch, T. B. H. & Procaccini, G. Local genetic structure in a clonal dioecious angiosperm. *Mol. Ecol.* **14**, 957–967 (2005).

26. Tuya, F., Espino, F. & Terrados, J. Preservation of seagrass clonal integration buffers against burial stress. *J. Exp. Mar. Bio. Ecol.* **439**, 42–46 (2013).

27. Terrados, J., Duarte, C. M. & Kenworthy, W. J. Is the apical growth of Cymodocea nodosa dependent on clonal integration? *Mar. Ecol. Prog. Ser.* **158**, 103–110 (1997).

28. Sánchez-Fernández, O., Marcos, C., Puerta, P., Sala-Mirete, A. & Pérez-Ruzafa, A. Spatial and Temporal Scales of Variability of Mollusks in a Strongly Threatened Mediterranean Coastal Lagoon (Mar Menor, Murcia, Spain). *Water (Switzerland)* **17**, 657 (2025).

29. Platt, T. *et al.* Photoinhibition of photosynthesis in natural assemblages of marine phytoplankton. *J. Mar. Res.* **38**, (1980).

30. Vásquez-Elizondo, R. M. *et al.* Absorptance determinations on multicellular tissues. *Photosynth. Res. 2017 1323* **132**, 311–324 (2017).

31. Collier, C. J., Uthicke, S. & Waycott, M. Thermal tolerance of two seagrass species at contrasting light levels: Implications for future distribution in the Great Barrier Reef. *Limnol. Oceanogr.* (2011) doi:10.4319/lo.2011.56.6.2200.

32. Collier, C. J., Ow, Y. X., Langlois, L. & Uthicke, S. Optimum Temperatures for Net Primary Productivity of Three Tropical Seagrass Species. **8**, 1–14 (2017).

33. Lichtenthaler, H. K. & Wellburn, A. R. Determinations of total carotenoids and chlorophylls a and b of leaf extracts in different solvents. *Biochem. Soc. Trans.* **11**, 591–592 (1983).

34. Smith, T., Heger, A. & Sudbery, I. UMI-tools: Modeling sequencing errors in Unique Molecular Identifiers to improve quantification accuracy. *Genome Res.* **27**, 491–499 (2017).

35. Ewels, P., Magnusson, M., Lundin, S. & Käller, M. MultiQC: summarize analysis results for multiple tools and samples in a single report. *Bioinformatics* **32**, 3047–3048 (2016).

36. Krueger, F. & Andrews, S. R. Bismark: a flexible aligner and methylation caller for Bisulfite-Seq applications. *Bioinformatics* **27**, 1571 (2011).

37. Akalin, A. *et al.* MethylKit: a comprehensive R package for the analysis of genome-wide DNA methylation profiles. *Genome Biol.* **13**, 1–9 (2012).

38. Bairoch, A. & Apweiler, R. The SWISS-PROT protein sequence database and its supplement TrEMBL in 2000. *Nucleic Acids Res.* **28**, 45 (2000).

39. Camacho, C. *et al.* BLAST+: architecture and applications. *BMC Bioinforma. 2009 101* **10**, 1–9 (2009).

40. Grossmann, S., Bauer, S., Robinson, P. N. & Vingron, M. Improved detection of overrepresentation of Gene-Ontology annotations with parent–child analysis. *Bioinformatics* **23**, 3024–3031 (2007).

41. Krzywinski, M. *et al.* Circos: an information aesthetic for comparative genomics. *Genome Res.* **19**, 1639–1645 (2009).

42. Pilar, A., González, R., Preite, V. & Verhoeven, K. J. F. Transgenerational Effects and Epigenetic Memory in the Clonal Plant Trifolium repens. **9**, 1–11 (2018).

43. Verhoeven, K., Jansen, J., van Dijk, P. & Biere, A. Stress-induced DNA methylation changes and their heritability in asexual dandelions. *New Phytol.* **185**, 1108–1118 (2010).

623 44. Verhoeven, K. J. F. & Preite, V. Epigenetic variation in asexually reproducing organisms. *Evolution*
624 *(N. Y).* **68**, 644–655 (2014).

625 45. Ding, Y. *et al.* Abiotic stress-induced DNA methylation in transposable elements and their transcripts
626 reveals a multi-layered response in Moso bamboo. *Ind. Crops Prod.* **210**, 118108 (2024).

627 46. Lee, J. *et al.* Distinct regulatory pathways contribute to dynamic CHH methylation patterns in
628 transposable elements throughout Arabidopsis embryogenesis. *Front. Plant Sci.* **14**, 1204279 (2023).

629 47. Pazzaglia, J. *et al.* Priming for seagrass resilience: DNA methylation and transcriptomic insights into
630 heat stress memory in Posidonia oceanica seedlings. *New Phytol.* **247**, 1156–1171 (2025).

631 48. Muyle, A. M., Seymour, D. K., Lv, Y., Huettel, B. & Gaut, B. S. Gene Body Methylation in Plants:
632 Mechanisms, Functions, and Important Implications for Understanding Evolutionary Processes.
633 *Genome Biol. Evol.* **14**, (2022).

634 49. Takuno, S. & Gaut, B. S. Gene body methylation is conserved between plant orthologs and is of
635 evolutionary consequence. *Proc. Natl. Acad. Sci.* **110**, 1797–1802 (2013).

636 50. Entrambasaguas, L., Ruocco, M., Verhoeven, K. J. F., Procaccini, G. & Guirao, L. M. Gene body
637 DNA methylation in seagrasses : inter - and intraspecific differences and interaction with
638 transcriptome plasticity under heat stress. *Sci. Rep.* 1–15 (2021) doi:10.1038/s41598-021-93606-w.

639 51. Deguette, A., Barrote, I. & Silva, J. Physiological and morphological effects of a marine heatwave on
640 the seagrass Cymodocea nodosa. *Sci. Rep.* **12**, 1–14 (2022).

641 52. Van Antro, M. *et al.* DNA methylation in clonal duckweed (Lemna minor L.) lineages reflects current
642 and historical environmental exposures. *Mol. Ecol.* **32**, 428–443 (2023).

643 53. Jueterbock, A. *et al.* The Seagrass Methylome Is Associated With Variation in Photosynthetic
644 Performance Among Clonal Shoots. *Front. Plant Sci.* **11**, 1 (2020).

645 54. Bewick, A. J. & Schmitz, R. J. Gene body DNA methylation in plants. *Current Opinion in Plant*
646 *Biology* vol. 36 103–110 at https://doi.org/10.1016/j.pbi.2016.12.007 (2017).

647 55. Waterworth, W. M., Latham, R., Wang, apeng, Alsharif, M. & West, C. E. Seed DNA damage
648 responses promote germination and growth in Arabidopsis thaliana. *Proc. Natl. Acad. Sci. U. S. A.*
649 **119**, e2202172119 (2022).

650 56. Pagano, A., De Sousa Araújo, S., Macovei, A., Leonetti, P. & Balestrazzi, A. The seed repair
651 response during germination: Disclosing correlations between DNA repair, antioxidant response, and
652 chromatin remodeling in medicago truncatula. *Front. Plant Sci.* **8**, 296775 (2017).

653 57. Moir, R. D. & Willis, I. M. Regulation of Pol III Transcription by Nutrient and Stress Signaling
654 Pathways. *Biochim. Biophys. Acta* **1829**, 361 (2012).

58. Pascali, C. & Teichmann, M. RNA polymerase III transcription - regulated by chromatin structure and regulator of nuclear chromatin organization. *Subcell. Biochem.* **61**, 261–287 (2013).

59. Meza, T. J. *et al.* The DNA dioxygenase ALKBH2 protects Arabidopsis thaliana against methylation damage. *Nucleic Acids Res.* **40**, 6620–6631 (2012).

60. Qiu, J. *et al.* Genome-Wide Analysis of the Protein Phosphatase 2C Genes in Tomato. *Genes (Basel).* **13**, 604 (2022).

61. Lawrence-Paul, E. H. & Lasky, J. R. Ontogenetic changes in ecophysiology are an understudied yet important component of plant adaptation. *Am. J. Bot.* **111**, (2024).

62. Rinaldi, A. *et al.* The ontogeny-specific thermal sensitivity of the seagrass Posidonia oceanica. *Front. Mar. Sci.* **10**, 1–11 (2023).

63. Ruocco, M. *et al.* A king and vassals' tale: molecular signatures of clonal integration in *Posidonia oceanica* under chronic light shortage. *J. Ecol.* 1365-2745.13479 (2020) doi:10.1111/1365-2745.13479.

64. Schwarzschild, A. C. & Zieman, J. C. Effects of physiological integration on the survival and growth of ramets and clonal fragments in the seagrass Syringodium filiforme. *Mar. Ecol. Prog. Ser.* **372**, 97–104 (2008).

65. Vieira, V. M. N. C. S. *et al.* Seagrass space occupation efficiency is key for their role as ecosystem engineers and ecological indicators. *Commun. Earth Environ. 2024 51* **5**, 592- (2024).

66. Yang, Y., Wang, W., Chu, Z., Zhu, J. K. & Zhang, H. Roles of nuclear pores and nucleo-cytoplasmic trafficking in plant stress responses. *Front. Plant Sci.* **8**, 264599 (2017).

67. Ravet, K. *et al.* Ferritins control interaction between iron homeostasis and oxidative stress in Arabidopsis. *Plant J.* **57**, 400–412 (2009).

68. Junaid, M. D., Chaudhry, U. K., Şanlı, B. A., Gökçe, A. F. & Öztürk, Z. N. A review of the potential involvement of small RNAs in transgenerational abiotic stress memory in plants. *Funct. Integr. Genomics 2024 242* **24**, 74- (2024).

69. Xu, W. B., Cao, F., Liu, P., Yan, K. & Guo, Q. H. The multifaceted role of RNA-based regulation in plant stress memory. *Front. Plant Sci.* **15**, 1387575 (2024).

70. Vittorioso, P., Cowling, R., Faure, J.-D., Caboche, M. & Bellini, C. Mutation in the Arabidopsis PASTICCINO1 Gene, Which Encodes a New FK506-Binding Protein-Like Protein, Has a Dramatic Effect on Plant Development. *Mol. Cell. Biol.* **18**, 3034 (1998).

Acknowledgements

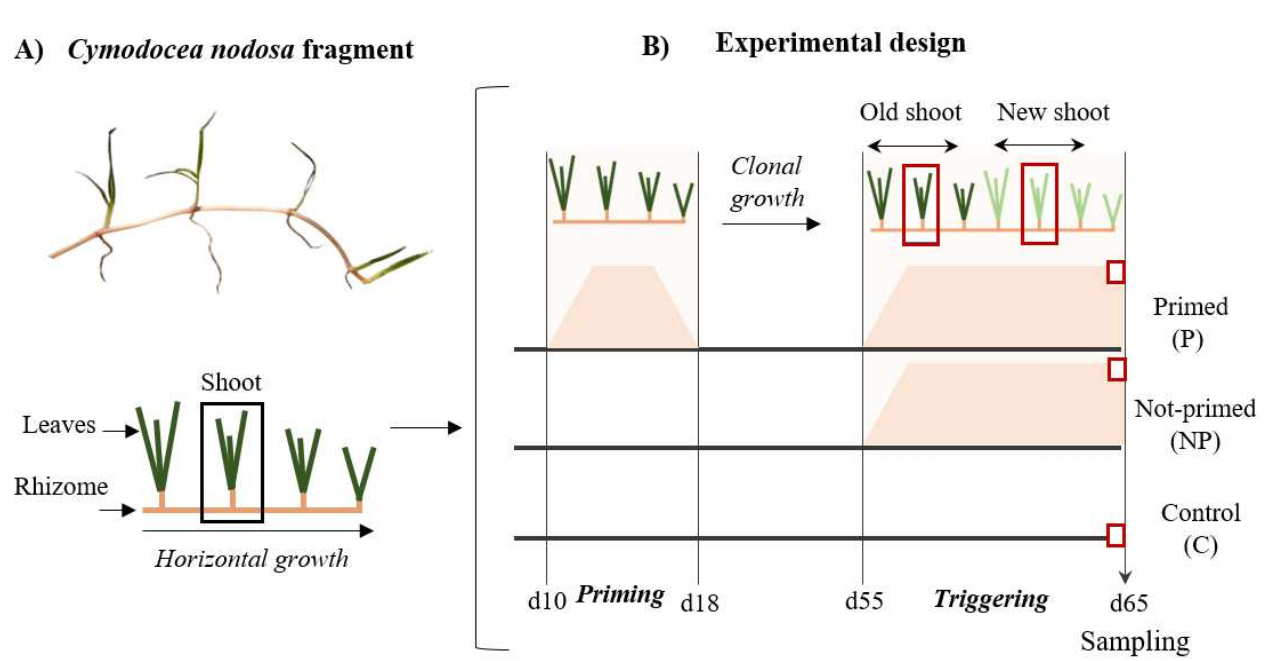
We are grateful to technicians who operated the vessel and assisted during sampling activities, and to Rocío García Muñoz for assistance during the PAM measurements. The work was supported by the project SMEMORY funding by National Geographic Society (NGS- EC-93498R-22), by the GRASSREC project (PID2020-118144RB-C31) of the Spanish Ministry of Science and Innovation, and partially by the project Marine Hazard, PON03PE_00203_1 (Ministry of Education, University and Research, MUR, Italy). The authors also acknowledge the ThinkInAzul Programme (C17.I01 – Complementary Plan for Marine Sciences, Region of Murcia), supported by MCIU with funding from the European Union NextGenerationEU (PRTR-C17.I1) and by the Comunidad Autónoma de la Región de Murcia–Fundación Séneca, for funding the upgrade of the mesocosm facilities used to conduct the experiments presented in this study. JP and GP received funding from the National Recovery and Resilience Plan (NRRP), Mission 4 Component 2 Investment 1.4 511 - Call for tender No. 3138 of 16 December 2021, rectified by Decree n.3175 of 18 December 2021 of Italian Ministry of University and Research funded by the European Union – NextGenerationEU (project code CN_00000033, Concession Decree No. 1034 of 17 June 2022 adopted by the Italian Ministry of University and Research, CUP C63C22000520001, Project title “National Biodiversity Future Center - NBFC”). LMG was partially supported by the GRASSREC 683 project, PID2020-118144RB-C31 (Spanish Ministry of Science and Innovation). The University of Calabria Ph.D. fellowship of FS was supported by Centro Ricerche ed Infrastrutture Marine Avanzate in Calabria (CRIMAC), Stazione Zoologica Anton Dohrn (MIUR Directoral Decree No. 388 of 23 March 2020).

Contributions

Conceptualization: J.P., G.P., L.M.G.; methodology: J.P., L.M.G., F.S, S.M, A.R.S; investigation: J.P, L.A; visualization: J.P, L.A.; funding acquisition: J.P, G.P, L.M.G., J. M. R.; writing original draft: J.P.; writing–review and editing: J.P, G.P, L.M.G, E. D., L.A.

Data availability

Raw bisulfite sequencing data have been deposited in the NCBI Sequence Read Archive (SRA) under accession number XXXXX.



721

722 **Figure 1. *C. nodosa* fragments and experimental design. (A)** Fragment of *Cymodocea nodosa* consisting of
723 an horizontal rhizome that enables clonal growth, with four/five shoots including the apical (runner) shoot,
724 each composed of leaves. Each shoot represents a ramet of the same genetic individual (clone) (See the main
725 text for more details). **(B)** Experimental design: *C. nodosa* fragments were first exposed to a priming phase
726 and then returned to control conditions to allow the growth of new shoots. Both old shoots (exposed to priming)
727 and newly developed shoots after priming were subsequently exposed to the triggering phase. Leaf samples
728 for analysis were collected at the end of triggering phase, before returning to control conditions, in primed (P),
729 not-primed (NP) and control (C) treatments. During sampling, both old shoots (exposed to priming and
730 triggering) and new shoots (exposed to triggering) were collected across treatments.

731

732

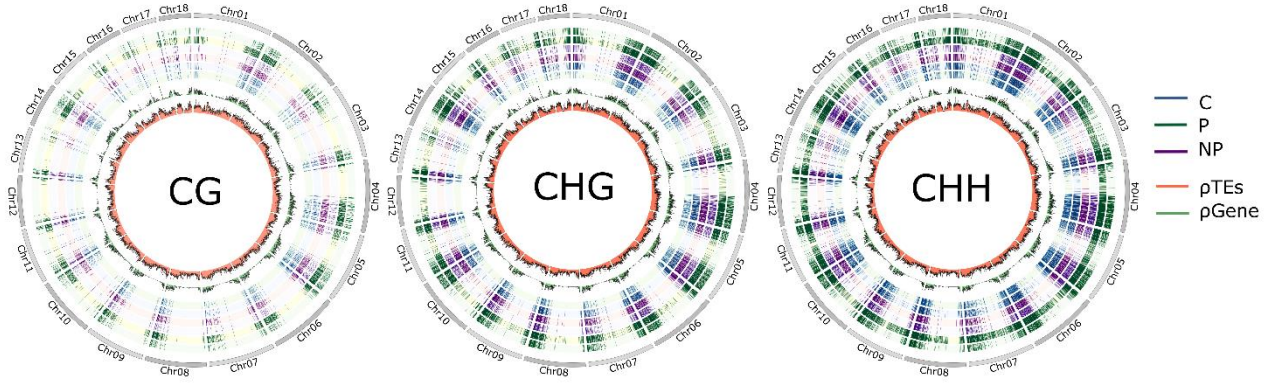
733

734

735

736

737



738

739 **Figure 2. Genome-wide DNA methylation landscapes**. Circular genome plots showing genome-wide DNA
740 methylation patterns across all chromosomes for the three cytosine sequence contexts (CG, CHG and CHH).
741 In each Circos plot, chromosomes are displayed as outer grey ideograms. Concentric heatmap tracks
742 represent normalized DNA methylation levels (50 kb resolution) for the six experimental conditions. From
743 the outermost to the innermost heatmap track, the conditions are displayed in the following order: primed
744 new, primed old, not primed new, not primed old, control new, and control old. Methylation values were
745 normalized within each cytosine context to a common 0–100 scale to enable direct comparison across
746 conditions. Inner histogram tracks (outermost to the innermost) indicate the gene density (ρGene) and
747 transposable element density (ρTEs) calculated over the same genomic windows. Color scales is reported in
748 the figure legend.

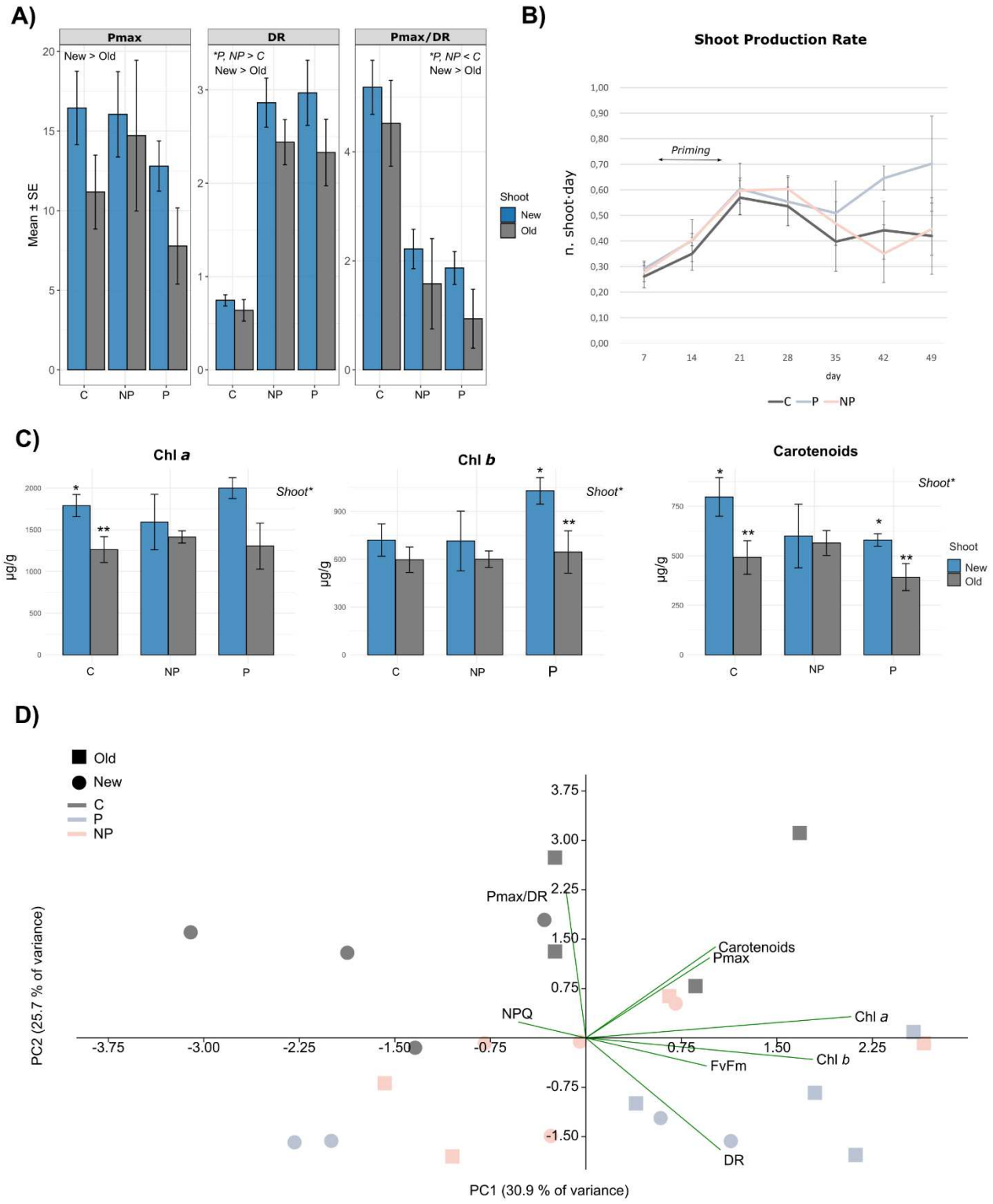


Figure 3. Plant traits responses in primed and not-primed conditions. (A) Bar plots showing maximum photosynthetic rate (Pmax), dark respiration (DR), and the Pmax/DR ratio measured in new and old shoots under Control (C), Primed (P), and Not-Primed (NP) conditions. Values are shown as mean ± standard error (SE). Error bars represent SE. Differences between new and old shoots within each treatment are indicated; asterisks denote statistically significant differences. **(B)** Shoot production rate measured throughout the experiment, prior to the triggering event, under Control (C), Primed (P), and Not-Primed (NP) conditions.

Values are shown as mean ± SE. **(C)** Bar plots reporting Chlorophyll a (Chl a), Chlorophyll b (Chlb, and Carotenoids content in new and old shoots under Control (C), Primed (P), and Not-Primed (NP) conditions. Values are shown as mean ± SE. Differences between new and old shoots within each treatment are indicated; asterisks denote statistically significant differences. D) Principal Component Analyss (PCA) based on different plats traits (Maximum photosynthetic, Pmax; dark respiration, DR; Pmax/DR ratio; photochemical efficiency, Fv/Fm; non-phochemical quenching, NPQ; chlorophyll a, Chl a; chlorophyll b, Chl b) and Differentially methylated regions (DMR_CG, DMR_CHG; DMR_CHH) averaged and visualized n=4. Statistical differences in panels A and C were assessed using two-way ANOVA (Treatment: Control, Primed, Not-Primed; Shoot type: New vs Old), followed by Tukey's HSD post hoc test where appropriate (Table S4). Panel B was analysed using one-way ANOVA testing the effect of Treatment (Control, Primed, Not-Primed), followed by Tukey's HSD post hoc test where significant (Table S8). Significant effects are reported at $p < 0.05$.

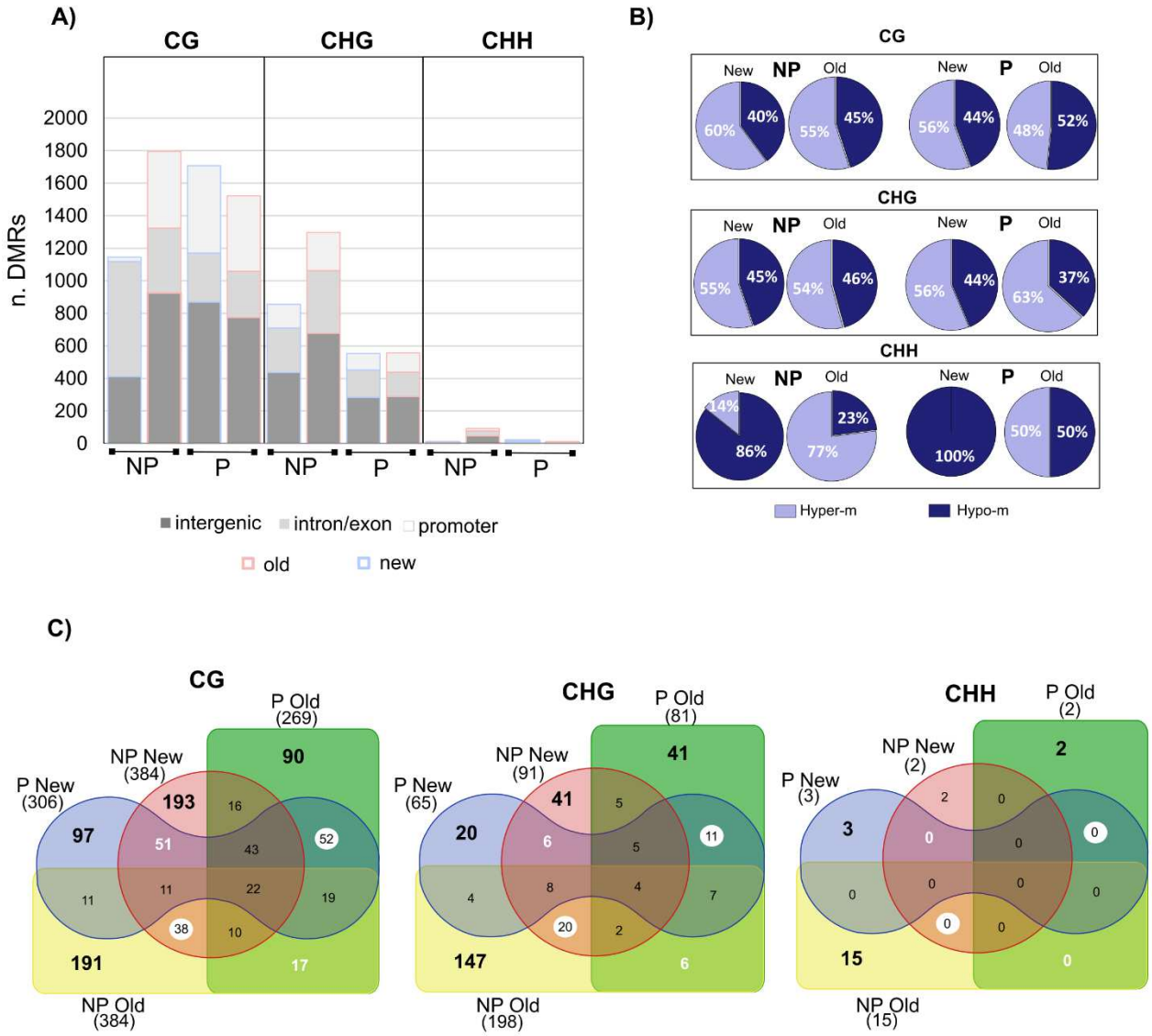
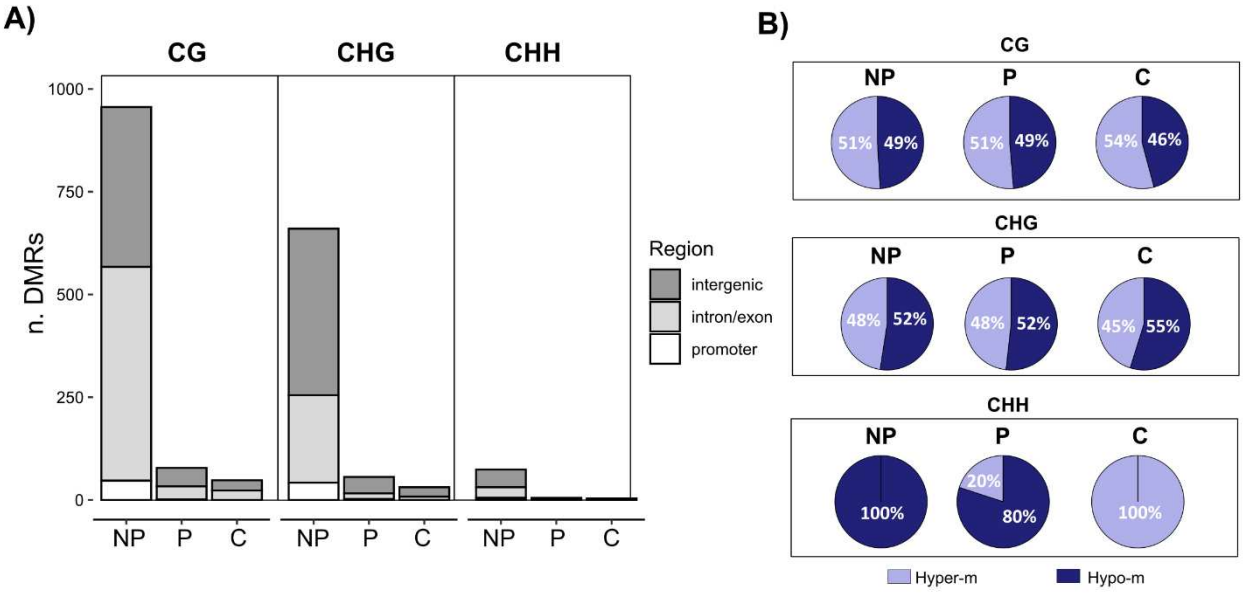
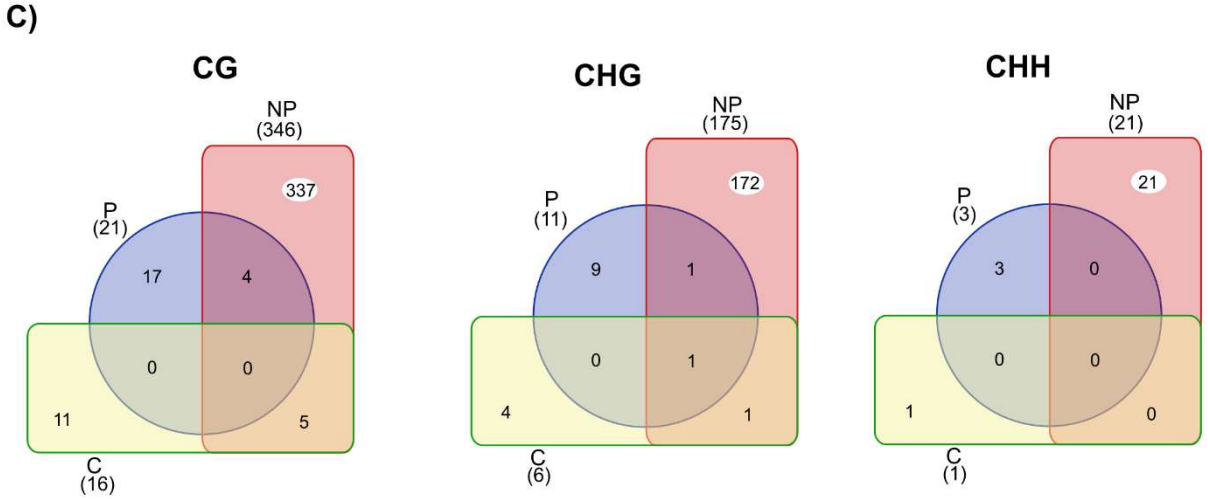


Figure 4. Differentially methylated regions (DMRs) in primed and not-primed conditions. **A)** Bar plots showing the total number of DMRs observed in primed (P) and not-primed (NP) conditions in different shoot types (new and old) across sequence contexts (CG, CHG, CHH). **B)** Pie charts representing the proportion of hypermethylated (Hyper-m) and hypomethylated (Hypo-m) DMRs in primed (P) and not-primed (NP) conditions, separated by shoot type (old and new). **C)** Asymmetric venn diagrams showing shared and unique annotated DMRs located within promoter and intron/exon regions between primed and not-primed conditions for each sequence context (CG, CHG, CHH). DMRs shown in these panels were identified by comparing each treatment (P and NP) with their respective controls. See the main text for further details.


A)
CG
CHG
CHH
n. DMRs
1000
750
500
250
0
NP
P
C
Region
intergenic
intron/exon
promoter
B)
CG
NP
P
C
51%
49%
51%
49%
54%
46%
CHG
48%
52%
48%
52%
45%
55%
CHH
100%
20%
80%
100%
Hyper-m
Hypo-m


C)
CG
NP
(346)
337
P
(21)
17
4
0
0
11
5
C
(16)
CHG
NP
(175)
172
P
(11)
9
1
0
1
4
1
C
(6)
CHH
NP
(21)
21
P
(3)
3
0
0
0
1
0
C
(1)

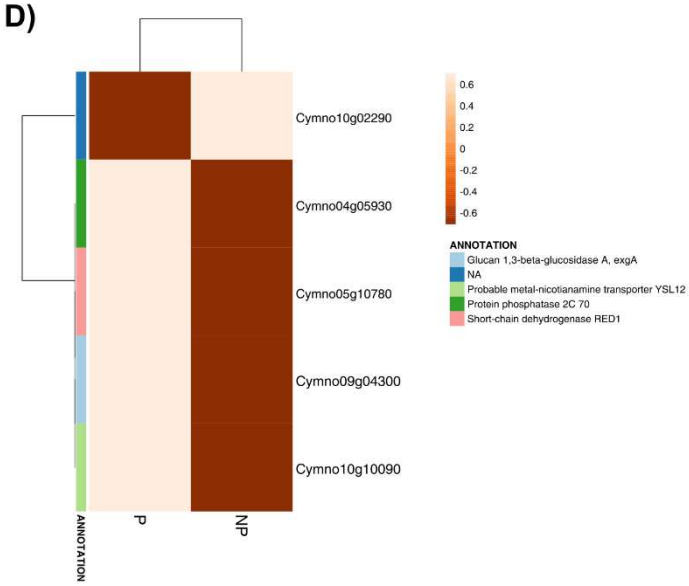

D)
Cymno10g02290
Cymno04g05930
Cymno05g10780
Cymno09g04300
Cymno10g10090
P
NP
ANNOTATION
0.6
0.4
0.2
0
-0.2
-0.4
-0.6
ANNOTATION
Glucan 1,3-beta-glucosidase A, exgA
NA
Probable metal-nicotianamine transporter YSL12
Protein phosphatase 2C 70
Short-chain dehydrogenase RED1

Figure 5. Differentially methylated regions (DMRs) within shoots under primed and not-primed conditions. A) Bar plots showing the total number of DMRs observed in primed (P), not-primed (NP), and control (C) conditions between new and old shoots across sequence contexts (CG, CHG, CHH). Bars are subdivided into genomic annotation categories (intergenic, promoter, and intron/exon). **B**) Pie charts representing the proportion of hypermethylated (Hyper-m) and hypomethylated (Hypo-m) DMRs in primed (P), not-primed (NP), and control (C) conditions, between new and old shoots across sequence contexts (CG, CHG, CHH). **C)** Asymmetric Venn diagrams showing shared and unique annotated DMRs located within promoter and intron/exon regions between primed (P), not-primed (NP), and control (C) conditions for each sequence context (CG, CHG, CHH). **D)** Heatmap of selected commonly shared DMRs with functional annotation.

Supplementary Files

This is a list of supplementary files associated with this preprint. Click to download.

- Supplementaryinformation.pdf
- SupplementaryData4.xlsx
- SupplementaryData1.xlsx
- SupplementaryData5.xlsx
- SupplementaryData3.xlsx
- SupplementaryData2.xlsx
- COMMSBIO266476rs.pdf